Available online at www.sciencedirect.com
SCIENCE DIRECT®
Applied Geochemistry 19 (2004) 395–412
Applied Geochemistry
www.elsevier.com/locate/apgeochem

Past and present circulation of CO_2-bearing fluids in the crystalline Gran Paradiso Massif (Orco Valley, north-western Italian Alps): tectonic and geochemical constraints

E. Sacchi[a,b,*], A. Dematteis[c], P. Rossetti[a]

[a] *Dipartimento di Scienze Mineralogiche e Petrologiche, Università di Torino, via Valperga Caluso 35, 10125 Torino, Italy*
[b] *Dipartimento di Scienze della Terra, Università di Pavia, via Ferrata 1, 27100 Pavia, Italy*
[c] *SEA Consulting s.r.l., via Cernaia 27, 10121 Torino, Italy*

Received 7 October 2002; accepted 8 July 2003
Editorial handling by H. Armannsson

Abstract

In the Orco Valley, inside the Gran Paradiso Massif, 3 main fault systems are present: (*a*) E–W striking faults dipping at 45–60° to the N, (*b*) high-angle NW–SE striking faults, and (*c*) high-angle NE–SW to NNE–SSW striking faults. The E–W striking faults and the interposed NW–SE-faults appear to represent a cogenetic structural association related to a larger scale transtensional shear zone, while the NE–SW faults are probably inherited by an older discontinuous deformation stage. Breccia bodies or veins, mostly consisting of carbonate (siderite–ankerite ± calcite) + quartz with sulphide–Au mineralisation, recording a multistage mesothermal evolution, occur along both E–W and NW–SE fault systems. Three water types are recognised: type I, Ca^{2+}–HCO_3^- waters, with minor SO_4^{2-}; type II, (Ca^{2+}/Na^+)–HCO_3^- waters varying towards Na^+–(HCO_3^-/Cl^-) waters; and type III, Mg^{2+}–HCO_3^- waters. Type I and type III groundwaters are freshly recharged waters, only slightly exchanged with rocks. Type II includes waters which come into contact with carbonate fracture fillings, and geochemical modelling indicates that dissolution of carbonates along fractures is the main process controlling the groundwater chemistry. These waters evolve in a system open to uprising CO_2, and their strongly negative $\delta^{13}C_{CO_2}$ suggests a substantial organic component in the CO_2 discharge. In the past, CO_2-bearing fluids were likely responsible for the formation of Fe-bearing carbonate fracture fillings. The persistence through time of the CO_2 flux in the region has important implications for the reconstruction of the Alpine tectonic evolution and deep structure.

1. Introduction

The mineralogical, petrographical and geochemical composition of fracture fillings in crystalline rocks can provide valuable information to understand the mechanism of mineral formation, and for the reconstruction of the past fluid circulation (e.g., Blyth et al., 2000; Conti et al., 2001). In recent years, work performed in the context of the performance assessment of nuclear waste repositories has shown the importance of fracture fillings in controlling groundwater chemical composition and radionuclide migration (e.g., Reyes et al., 1998). These studies, allied with observed structural patterns, are determinants for the definition of groundwater flow patterns and residence time (Clauer et al., 1989; Gascoyne and Wikberg, 1999).

In 1999, AEM Torino S.p.A., owner of the Orco Valley hydropower plants (north-western Italian Alps), entrusted SEA Consulting with the task of carrying out a pre-feasibility geological study for the renewal of the existing plants. The study covered an area of about 300

* Corresponding author. Fax.: +39-0382-505-890.
E-mail address: elisa.sacchi@manhattan.unipv.it (E. Sacchi).

0883-2927/$ - see front matter © 2003 Elsevier Ltd. All rights reserved.
doi:10.1016/S0883-2927(03)00152-5

km^2, from the Agnel Lake to the Locana-Bardonetto area, and involved geological mapping (1:10.000 scale), and structural, hydrogeological and geomechanical analysis, in order to evaluate new hydraulic schemes and excavation techniques for diversion tunnels and powerhouse caverns (SEA Consulting, 2001).

This paper reports the results obtained on fracture fillings, and was aimed at defining a hydrogeological and geochemical model, by which deep-seated fluids are recognised in view of the excavation work.

2. Geological and hydrogeological setting

2.1. Regional geological setting

In the Orco Valley (Western Italian Alps, Fig. 1) 3 superimposed tectono-stratigraphic units, separated by syn-metamorphic ductile contacts, are present (Fig. 2). These are, from bottom to top, the Gran Paradiso Massif, the Piemontese Ophiolitic Unit and the Sesia-Lanzo Unit. These units show a composite metamorphic foliation developed under early high pressure alpine conditions related to a late Cretaceous to Paleocene oceanic subduction cycle, followed by a retrograde evolution towards low pressure conditions, which caused pervasive greenschist facies re-equilibration of the high pressure mineral associations, related to an Eocene to early Oligocene continental collision phase.

The Gran Paradiso Massif of the Penninic Domain in the mapped area (Fig. 2) is made up of late-Hercynian granitic gneisses derived from pre-alpine granitic intrusions in a metamorphic basement (paragneisses) containing relicts of the Hercynian metamorphism (Compagnoni and Prato, 1969; Compagnoni et al., 1974; Dal Piaz and Lombardo, 1986). The composite foliation in the Gran Paradiso Massif describes a dome shaped structure, that dips ESE in the eastern sector, WNW in the western sector and sub-horizontal in the unit's core (Delle Piane et al., 2001a,b). The Piemontese Ophiolitic Unit of the Penninic domain overlies the Gran Paradiso Massif, which is mainly composed of

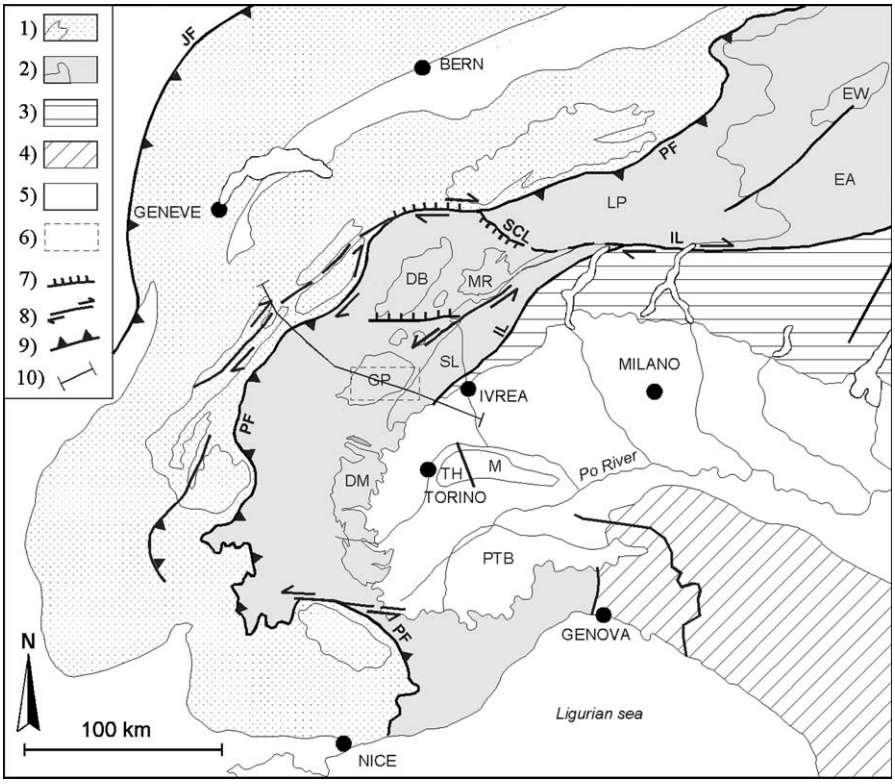

Fig. 1. Tectonic scheme of north western Alps. (1) Helvetic domain: Mesozoic/Cenozoic Covers and main outcrops of European basement; (2) tectonic Units of the Alpine accretionary wedge (Penninic, Austroalpine, Briançonnais): EA = Eastern Austroalpine, EW = Engadine Window, LP = Lower Penninic nappes, MR = Monte Rosa nappe, DB = Dent Blanche nappe, SL = Sesia Lanzo unit, GP = Gran Paradiso massif, DM = Dora Maira massif; (3) South Alpine units; (4) Apennines; (5) Oligocene and Neogene synorogenic sedimentary deposits: TH = Torino Hill, M = Monferrato, PTB = Piedmont Tertiary Basin; (6) Location of the studied area; (7) Normal faults. SCL: Simplon-Centovalli Line; (8) Strike-slip faults. IL: Insubric Line; (9) Thrust faults. JF = Jura Front, PF = Penninic Frontal thrust.

calcschists, marbles, serpentinised peridotites, metabasites and metagabbros. Its composite regional foliation is pervasively developed, and mainly parallel to the ductile contacts with the Gran Paradiso Massif, dipping toward ESE in the eastern sector and WNW in the western sector. The Sesia-Lanzo Unit of the Austroalpine domain only crops out in a limited portion of the mapped area and is mainly composed of gneisses. The contact with the Piemontese Ophiolitic Unit is a ductile tectonic contact composed of interbedded decametric to hectometric slices of the two units.

2.2. Brittle deformation

Inside the Gran Paradiso Massif, fault and fracture systems cut across the low-angle to medium-angle composite ductile schistosity of the gneisses, producing only minor and local cataclastic reactivation. Mapped faults display a great degree of segmentation and their growth does not seem to be conditioned by the pre-existing foliation. Three fault systems have been identified at the mesoscopic scale (Perello et al., submitted for publication):

- E–W striking faults dipping at 45–60° to the N;
- high-angle NW–SE striking faults; and
- high-angle NE–SW to NNE–SSW striking faults.

In all these systems the main fault products are breccias, often affected by argillification, along with rare cataclasites. The thickness of tectonic breccias generally varies from a few centimetres to approximately 5 m. The transition to the less fractured rock mass generally occurs through a belt of high fracture density, where the gneiss often displays a protobreccia structure at the micro-scale, due to shearing along the schistosity surfaces. The thickness of high degree of fracturing and protobreccia belts ranges from a few metres to 50 m. Meso-scale shear surfaces show mainly grooves and striae, but siderite and quartz slikensides are also widespread.

Both E–W and NW–SE systems show breccias sometimes cemented by siderite and ankerite. At some locations these minerals form breccia bodies or veins from a decimetre to a metre in thickness and are associated with sulphide and Au mineralisation (Cuccagna and Bellagarda mines: Fig. 2). In spite of this local evidence of paleo-hydrothermal activity, the prevailing feature is the absence of hydrothermal fluids during fault shearing. On the other hand, the NE–SW system is associated with extensional fractures locally affected by fluid circulation, which caused metasomatic alteration of the rock with development of albite, chlorite, hematite and magnetite. The NE–SW system is therefore related to hydrothermal phenomena, with fluid circulation probably occurring at higher temperature than in the other systems.

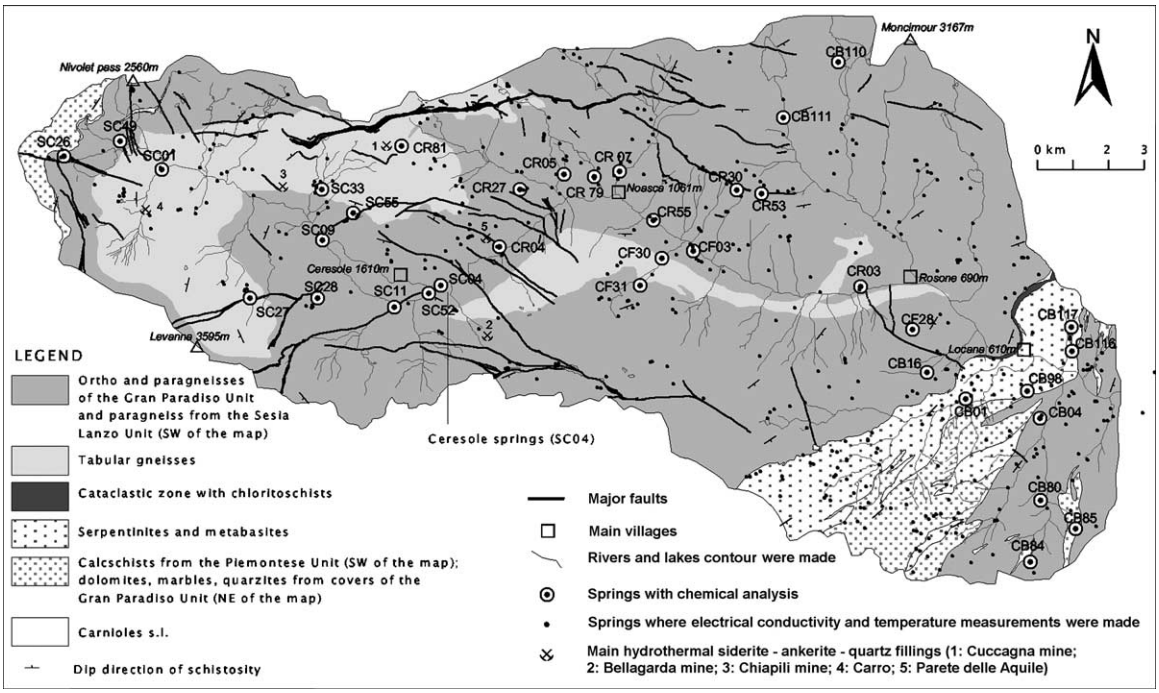

Fig. 2. Hydrogeological and structural map of the Orco Valley obtained from 1:10,000 field mapping, showing the location of sampled fracture fillings and springs.

The structural framework of these 3 fault systems appears to be dominated by two "through-going shear zones" belonging to the E–W system, displaying a lateral continuity of about 10 km (Fig. 2). They crop out at high altitudes on both sides of the Orco Valley. These shear zones originated by linkage of discrete minor faults striking ENE–WSW and ESE–WNW, and display a typical anatomised geometry of internal mesoscale structures. The thickness of the related breccia and protobreccia belt ranges from 100 to 200 m. Kinematic analysis of these shear zones indicates that they accommodated a right lateral shear component associated, in the last stages of deformation, with an oblique, normal component. The rock volume interposed between the two E–W shear zones is dominated by discrete faults of the NW–SE system with 2–3 km of lateral persistence. These are mainly right lateral and normal faults. The authors interpreted the two E–W through-going shear zones and the interposed NW–SE faults as a co-genetic structural association; the NW–SE discrete faults are synthetic Riedel shears of a larger scale transtensional shear zone bordered by the two E–W through-going faults. This large scale shear zone does not seem to produce an important displacement of the tectonic contacts bordering the Gran Paradiso Massif. Therefore it could represent a strain accommodation feature internal to the massif rather than a regional discontinuity.

NE–SW faults are mainly normal faults which are not compatible with the E–W shear zone. They were probably inherited from an older discontinuous deformation stage related to slightly deeper crustal levels, as is also suggested by field relationships and phase assemblages. Similarly, many NW–SE faults display an oblique reverse and left-lateral shearing pre-dating the transtension along the E–W shear zone, thus attesting to the presence of a pre-existing compressional regime in the massif.

The features described above suggest that, contrary to the classical cartographic representations (Compagnoni et al., 1974), the Gran Paradiso Massif underwent a complex and polyphase evolution within a discontinuous deformation field. Nevertheless, structural analysis indicates that only minor strain was accommodated inside the massif.

2.3. Fracture mineral fillings

As already mentioned, hydrothermal mineral fillings occur along the E–W and NW–SE fault systems, and consist mostly of carbonates and quartz. Sulphide (±Au) ores have been locally mined, during the past two centuries, both in the Orco Valley (Cuccagna, Bellagarda mines: Fig. 2) and in other sectors of the Gran Paradiso Massif (Cevales, 1961). At mesoscopic scale, fillings occur as veins or lens-shaped bodies within the fracture systems, with thickness ranging from a centimetre to a metre, and show a variety of structures and mineralogical compositions. Field relationships indicate that the carbonate fillings postdate the albite-bearing assemblage observed in the NE–SW fault system.

Massive veins are common and typically consist of coarse grained siderite with minor quartz, the latter often concentrated at vein walls. They display a poorly developed banded structure, due to the increase of quartz towards the outer portions. Quartz is often present as euhedral crystals up to few centimetres long, perpendicular to the vein wall ("comb texture"). Within the veins, cockade structures occur when hydrothermal fillings cement a preexisting breccia along the fracture plane: in this case, orthogneiss clasts are surrounded by a millimetre-thick rim of quartz, embedded within the siderite matrix. Ankerite is another important mineral within the hydrothermal fillings. Field relationships show that ankerite deposition is related to a separate and later hydrothermal stage, as it occurs as a fine grained matrix cementing up to decimetre-sized clasts composed of siderite and quartz. Ore minerals, which are typically absent in siderite + quartz portions, often occur and can become important in ankerite-rich domains, thus suggesting a relationship between this second hydrothermal stage and mineralisation. Both the siderite- and ankerite-rich domains are often crosscut by thin and irregular carbonate-rich veinlets. At the contact with the carbonate fillings, the orthogneiss host rock is affected by a centimetre-thick reddish halo of hydrothermal alteration. Apart from the carbonate fillings, millimetre-thick quartz ± sulphide veinlets occasionally occur along the same fracture systems (e.g., Cuccagna, Parete delle Aquile; Fig. 2). Clear relationships between these veinlets and the much more abundant carbonate-bearing assemblages have not been observed in the field.

Summing up, preliminary field observations allow the identification of features in veins (structural setting and banded, cockade and comb structures) which strongly suggest deposition from hydrothermal fluids within the dilation portions of the system. Also, field relationships suggest that the siderite–ankerite veins are a product of a multistage evolution, with an early, siderite-rich hydrothermal stage followed by a later ankerite-rich stage. Sulfide ores appear to be related to the later stage.

2.4. Hydrogeology

This geological study allowed the grouping of all the outcropping lithotypes into hydrogeological formations (Table 1), the latter being defined in terms of permeability (either porous or fissured) and degree of permeability (low, medium or high). Fig. 2 shows the hydrogeological map of the valley, where only the hydrogeological formations of the basement are visible,

Table 1
Hydrogeological classification of the formations outcropping in the Orco Valley and their degree of permeability

Formations	Type of permeability	Degree of permeability		
		Low	Medium	High
Alluvial deposits	porous		X	
Slope debris deposits	porous			X
Glacial deposits	porous		X	
Calcschist and carbonatic rocks	fissured	X		
Serpentinites and metabasites	fissured		X	
Orthogneiss and gneiss from the Gran Paradiso Massif	fissured	X	X	

as the others are too small in dimension to be represented on this scale.

The groundwater flow in the Orco Valley is located in the Quaternary glacial and slope deposits, and in the basement. In the former, thin porous aquifers occur within mountain slopes. Alluvial deposits in the bottoms of the valleys are discontinuous and do not hold important water resources.

The basement is a fissured permeable medium where the permeability field is anisotropic on all scales and heterogeneous, due to the highly ductile and brittle nature of the rock. In general, the groundwater flow systems are small, and often occupy only a part of the valley slope, down to a depth of 50–100 m from the surface. Some flow systems are deeper and more extended, like the Ceresole one.

The hydrogeological reference model for the Orco Valley, based on field mapping and on the geochemical results discussed below, is shown in Fig. 10. Two main types of groundwater flow systems are distinguished:

1. Rapid groundwater flow systems. These are shallow flow systems (a few tens of metres), and are developed both in the weathered zone of the Massif, near the surface, and in thin Quaternary deposits. The groundwater recharge is local and comes from the upper parts of the slope. This type of system feeds most of the springs observed in the Orco Valley. The springs have a mean discharge lower than 0.5 l/s. Waters have a low TDS, and an electrical conductivity ranging from 10 to 100 μS cm^{-1}.
2. Deep groundwater flow systems. These extend to the scale of the whole Massif. They are located in faults and other discontinuities in the rock basement and can reach depths of more than a hundred meters. These are recently recharged descending waters, percolating from high elevation and outflowing at the bottom of the valley at the hydraulic minimum. The waters are medium to highly mineralised with electrical conductivity above 100 and up to 1500 μS cm^{-1}. In extreme cases, as for instance at Ceresole, springs display effervescence and Fe oxy-hydroxides precipitate around the outflow.

3. Sampling and analytical methods

Following an extensive regional geological survey, fracture filling samples were collected at different locations within the Gran Paradiso Massif (Fig. 2). Mineralogical determinations were carried out at the University of Torino, using optical microscopy (both transmitted and reflected light), cathodoluminescence, X-ray powder diffraction (XRD), and scanning electron microscopy. Oxygen and carbon isotope analysis of carbonates was performed by ISO4 s.s., Torino, using the selective acid extraction described by Al-Aasm et al. (1990). All values are expressed in δ ‰ notation relative to PDB (Craig, 1957). The isotopic composition of siderite and ankerite were obtained by reaction with phosphoric acid at higher temperatures and recalculated to 25 °C taking into account the fractionation factors for acid decomposition reported by Rosenbaum and Sheppard (1986).

In order to test the possible contribution of fracture fillings to groundwater salinity, leaching experiments were performed. Samples were finely crushed in an agate mortar, mixed with deionised water at different water–rock ratios, and allowed to stand for 72 h at room temperature. Leachates were extracted by centrifugation and analysed using the techniques described below.

Water samples from springs were collected during two separate campaigns in autumn 1999 and 2000, at the minimum groundwater level. The sampling locations were chosen in order to homogeneously cover the territory and to be representative of the different aquifers (Fig. 2). The pH, redox potential, alkalinity (by HCl titration) and conductivity were in most cases measured in situ. Samples were subsequently filtered through 0.45–μm membrane filters and collected in pre-cleaned bottles. A sample aliquot was acidified to 1% HNO_3 for

the analysis of cations and metals. Major and trace elements were analysed at the LARA s.r.l. laboratory, Torino (1999 campaign) and at the University of Torino (2000 campaign). Anions were determined by ion chromatography. Cations and trace elements were determined by inductively coupled plasma atomic emission spectroscopy (ICP–AES).

Samples for stable isotope analysis and ^{3}H were collected in the second campaign according to the procedures described by Clark and Fritz (1997). Isotopic ratio analyses for H, O and C were performed at ISO4 s.s., Torino. Hydrogen isotope composition was measured by water reduction over metallic Zn (Coleman et al., 1982), while $\delta^{18}O$ was analysed by water–CO_2 equilibration at 25 °C (Epstein and Mayeda, 1953); both results are expressed in δ‰ SMOW (Standard Mean Ocean Water). The $\delta^{13}C$ of DIC was analysed by direct acidification of the water sample with phosphoric acid (Kroopnick, 1974). These results are expressed in δ ‰ PDB (Craig, 1957). All gases were analysed on a *Finnigan*™ MAT 250 Mass Spectrometer. Tritium was measured by β^{-} counting after electrolytic enrichment at Hydroisotop GmbH, München, and results are expressed in Tritium Units (1 T.U. corresponding to $^{3}H/H = 10^{-18}$) (Unterweger et al., 1980).

Dissolved gas analysis was performed on one water sample only, by gas chromatography at the IGGI-CNR, Pisa, with a Carlo Erba 5320 gas chromatograph equipped with a thermal conductivity detector and using ultra pure He as gas carrier.

4. Results

4.1. Fracture fillings

4.1.1. Petrography

The earliest association in carbonate fillings is represented by siderite and quartz. In this assemblage, siderite and quartz are typically medium to coarse grained; quartz occurs as euhedral crystals, often perpendicular to vein walls, and/or as clasts in portions showing cockade structure. Siderite is close to the end member composition (Fig. 3), and shows a range of $Fe^{+2}/(Fe^{+2}+Mg)$ (at.%) ratios between 0.79 and 0.92. It contains appreciable amounts of MnO (2.13–4.19 wt.%), as found for other syn- to late-orogenic hydrothermal siderite occurrences (e.g., Renish Massif: Hein, 1993; Lanzo Valleys, Italian Western Alps: Castelli et al., 1995). As already evident in the field, this early deposition stage has also been followed by a brittle deformation episode on a microscopic scale, accompanied by a second stage of fluid infiltration and mineral deposition.

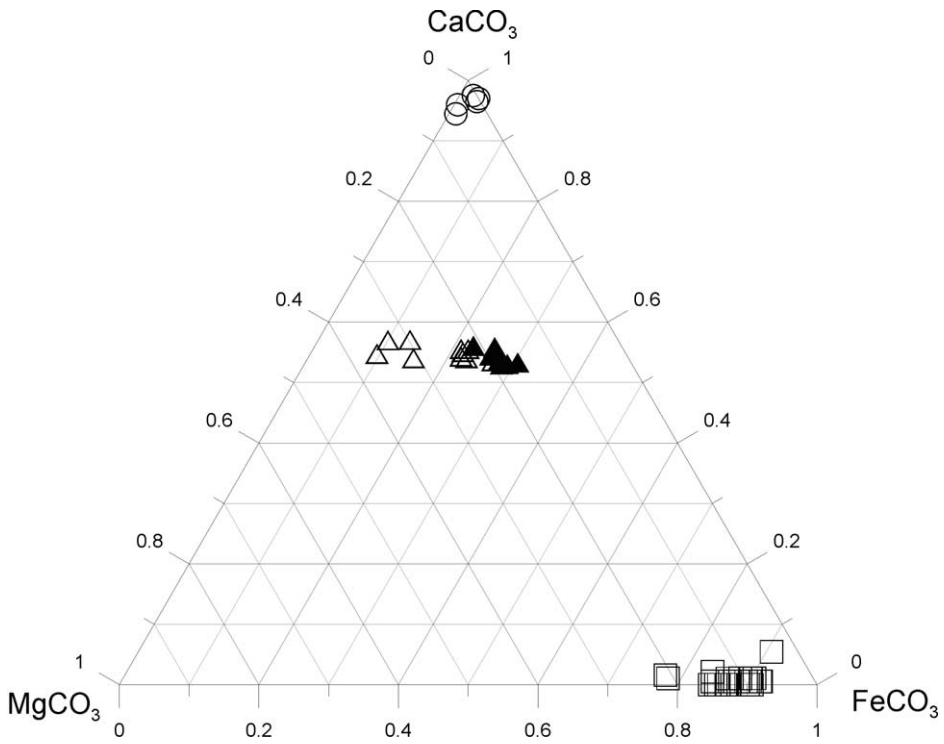

Fig. 3. Ternary composition plot of carbonates from the hydrothermal veins. Squares: siderite; filled triangles: ankerite I; open triangles: ankerite II; open circles: calcite.

The early siderite + quartz assemblage is brecciated, and occurs as angular clasts (ranging in size from a hundred microns to tens of centimetres) embedded in a finer grained matrix. The latter consists of rock flour, i.e. crushed siderite + quartz, along with a new hydrothermal filling mostly composed of ankerite (ankerite I), made up of medium to fine grained crystals characterised by a low MnO content (0.42–1.11 wt.%) and a relatively narrow compositional range, with a $Fe^{+2}/(Fe^{+2}+Mg)$ (at.%) ratio ranging from 0.52 to 0.65 (Fig. 3). Ankerite often occurs together with a variety of ore minerals, occurring as disseminations around the siderite clasts or along microfractures within siderite. The relative abundance of ore minerals is highly variable through the vein system; generally pyrite, arsenopyrite and tetrahedrite crystallise first, followed by the other metallic phases which include chalcopyrite, galena, jamesonite, sphalerite, bournonite, freibergite. Gold (actually electrum, $\sim Au_{0.8}Ag_{0.2}$) is quite common, mostly as a relatively late phase along microcracks in tetrahedrite, pyrite and arsenopyrite, where it is mostly associated with galena.

A third hydrothermal stage is at times represented by carbonate veinlets, a few microns to some millimetres thick, which crosscut the previously formed fillings. These veinlets are irregularly shaped and discontinuous, and consist of a new ankerite generation (ankerite II). Backscattered images and microprobe analyses show that ankerite II is characterised by strong compositional zoning on the micron scale. In the $CaCO_3$–$MgCO_3$–$FeCO_3$ ternary diagram (Fig. 3), its composition plots along the ankerite–dolomite binary and shows a highly variable $Fe^{+2}/(Fe^{+2}+Mg)$ (at.%) ratio, ranging from 0.21 (very close to dolomite) to 0.59.

The occurrence of very minor amounts of calcite within both the siderite + quartz domains and the ankerite matrix has been shown by cathodoluminescence and also been confirmed by SEM–EDS and XRD analyses. In the first case, calcite partially replaces strongly weathered siderite crystals, which are surrounded by abundant Fe (and subordinate Mn) hydroxides. In the second case, calcite occurs as thin rims around ankerite and as fine grained overgrowths inside the ankerite crystals often related to microcracks. Small calcite crystals—showing micron-sized growth zoning—also fill small vugs between the ankerite crystals. These relationships suggest that calcite crystallization represents a minor event, probably related to local, low temperature fluid circulation postdating the deposition of the main hydrothermal assemblages.

As already mentioned, apart from the carbonate fillings, thin quartz ± sulphide veinlets also occasionally occur along the same fracture systems. These veinlets consist of fine- to medium-grained intergrowths of sub-euhedral quartz crystals and variable amounts of sulphides (mainly arsenopyrite and pyrite). On a microscopic scale, the quartz-rich assemblage rarely occurs also as domains embedded in a siderite matrix, suggesting that it is the product of an early hydrothermal stage, which pre-dated carbonate deposition.

Hydrothermal alteration on the host orthogneiss is mainly represented by limited sericitisation and carbonation, often accompanied by addition of quartz ± pyrite. Such alteration appears to be related to the earliest (siderite + quartz) stage. The later hydrothermal stages do not show visible effects on the previously altered host rock and on the earlier vein assemblages.

4.1.2. Leachates

Four leachates of powdered fracture fillings were produced by treatment with MilliQ deionised water, in order to test the release of anions and cations during groundwater circulation. Obviously, this procedure is not suitable for obtaining direct information about the rock composition or about water–rock interactions (Sacchi et al., 2000). Results are reported in Table 2, together with the water–rock ratios and the back calculation to the rock content. Alkalinity was not measured as experiments were not conducted in a controlled atmosphere.

The amounts of leached Cl^- are high, and display in most cases a 1:1 molar ratio with Na. This suggests the presence of NaCl-bearing fluid inclusions (Savoye et al., 1998). Boron, Ba, Li and Sr are also present in the solution, but do not display fixed ratios with Cl^-, suggesting a release by partial dissolution of mineral phases rather than fluid inclusion leaching. Nitrate and K concentrations are also high, but their origin is not clear. Siderite-dominated fillings display a 1:1 molar ratio of Ca to Mg, while this ratio increases when ankerite and calcite are present. This is likely to be due to the difference in amount and solubility of carbonate minerals, although no further conclusion can be drawn due to lack of alkalinity data.

4.1.3. Stable isotopes

The results of isotope analysis of carbonates (siderite, ankerite I and calcite) from fracture fillings are reported in Table 3. Ankerite I shows intermediate isotopic contents relative to siderite and calcite. The siderite composition is very close to that reported by Hein (1993) and Cortecci and Frizzo (1993) for hydrothermal deposits and veins.

Isotopic geothermometers cannot be applied to mineral pairs because of the lack of evidence of co-precipitation among carbonates and the absence of published fractionation factors for ankerite. $\delta^{13}C$ values are negative, especially for Fe-rich carbonates, indicating a possible organic C contribution of CO_2, in agreement with what was suggested by Hein (1993).

Table 2
Chemical composition of leachates obtained on powdered fracture minerals at the indicated water-rock ratio (wt./wt.)

Sample	SEA 58		SEA 153		SEA 53		SEA 154	
Rock–water ratio	0.05204		0.02495		0.05005		0.10024	
Mineral phases	Ank > Sid > Qz		Sid > Qz > Ank > Crist > Calc		Sid > Qz		Sid > Qz > > Ank	
Aqueous leachates	Solution concentration mg/l	Extracted ions mg/kg	Solution concentration mg/l	Extracted ions mg/kg	Solution concentration mg/l	Extracted ions mg/kg	Solution concentration mg/l	Extracted ions mg/kg
Na^+	3.04	58.4	1.05	42.1	2.26	45.2	4.55	45.4
K^+	2.74	52.7	0.63	25.3	5.9	118	3.6	35.9
Ca^{2+}	16	311	13	533	16	312	17	167
Mg^{2+}	7.2	138	4.3	172	9.4	188	9.8	98
Cl^-	4.55	87.4	1.63	65.3	2.82	56.3	7	69.8
SO_4^{2-}	0.8	16	2	80	0.8	16	1.8	18
NO_3^-	0.2	3.8	4	160	5.6	112	0.7	6.5
B	0.11	2.11	n.m.	n.m.	n.m.	n.m.	n.m.	n.m.
Ba^{2+}	0.02	0.38	0.45	18	n.d.	n.d.	0.002	0.02
Li^+	0.04	0.77	n.d.	n.d.	n.d.	n.d.	n.d.	n.d.
Sr^{2+}	0.07	1.35	0.04	1.6	0.04	0.8	0.02	0.2

n.m. = not measured; n.d. = not detected.

4.2. Water samples

4.2.1. Chemical data

The conductivity and TDS values for most water samples (Table 4) are low, which could account for some uncertainties in the analyses, as evidenced by mass balance calculations (Fritz, 1994). Temperatures are normally below 10 °C, and testify to the absence of thermal waters. pH values range from close to neutrality to slightly acidic (7.9–5.5). Eh values are positive, except the negative value for the most saline sample SC04.

According to the classification of Jäckli (1970), three main types of water can be distinguished (see also Fig. 4):

- Type I: Ca^{2+}–HCO_3^-–(SO_4^{2-}) i.e. calcium–bicarbonate dominated waters, with minor sulphate waters;
- Type II: Ca^{2+}–Na^+–HCO_3^- waters varying to Na^+–HCO_3^-–Cl^- waters;
- Type II: Mg^{2+}–HCO_3^- waters

Table 3
Isotopic composition of fracture filling carbonates

Sample	Phase	$\delta^{13}C$ ‰ PDB	$\delta^{18}O$ ‰ PDB
53A	Calcite	−3.97	−21.24
53B	Ankerite	−7.76[a]	−19.27
53B	Siderite	−5.96	−13.50
53C	Siderite	−9.20	−12.94
153A	Siderite	−9.16	−13.30
153B	Ankerite	−7.30[a]	−11.78

[a] Values obtained by acid attack at 50 °C and not corrected to 25 °C because of the lack of published fractionation factors.

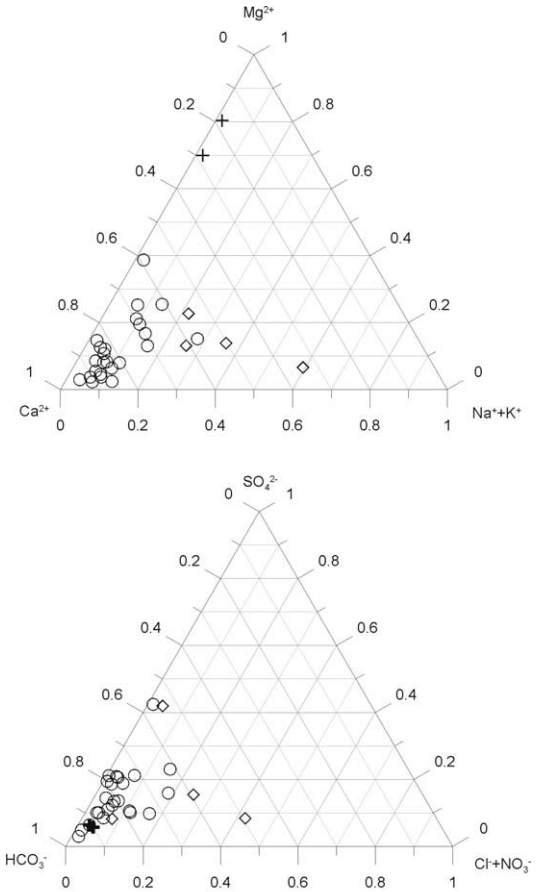

Fig. 4. Ternary composition plots of water samples. Open circles=Type I waters; open diamonds=Type II waters; crosses=Type III waters.

Table 4
Chemical composition of studied groundwaters. n.m. = not measured

Sample.	Year	Type	Outflow ($l\ sc^{-1}$)	Cond. ($\mu S\ cm^{-1}$)	T (°C)	pH	Eh (mV)	Na^+ (mg/l)	K^+ (mg/l)	Ca^{2+} (mg/l)	Mg^{2+} (mg/l)	Cl^- (mg/l)	HCO_3^- (mg/l)	SO_4^{2-} (mg/l)	NO_3^- (mg/l)	F^- (mg/l)	SiO_2 (mg/l)	As (μg/l)	Ba (μg/l)	B (μg/l)	Fe (μg/l)	Mn (μg/l)	Li (μg/l)	Sr (μg/l)	TDS (mg/l)
CB01	1999	I	0.5–2	82	11.3	6.9	n.m.	3.1	2.2	17	1.9	1.3	67.12	6.1	0.1	0.486	6	5	3.1	n.m.	6.8	0.9	n.m.	n.m.	105.3
CB04	1999	I	0.5–2	191	9.8	7.9	n.m.	2.3	2	42	1.6	1.3	97.63	58	0.1	2.41	4.8	5	1.3	n.m.	58	0.78	n.m.	n.m.	212.2
CB16	1999	I	2–10	20	7.7	5.9	n.m.	2	0.39	0.5	0.29	0.2	3.05	5.2	2.8	0.158	6	5	1.5	n.m.	1	0.29	n.m.	n.m.	20.6
CB84	1999	I	0.5–2	n.m.	n.m.	n.m.	n.m.	2.1	0.22	21	0.66	0.32	30.5	3.2	6.5	0.1	5.6	5	4.8	n.m.	7.1	1.3	n.m.	n.m.	70.2
CB98	1999	I	2–10	148	10.1	6.9	n.m.	2.5	0.85	31	1.8	0.61	73.22	14	20	0.1	7.2	5	7.6	n.m.	1	0.5	n.m.	n.m.	151.3
CF03	1999	I	>10	50	8.9	n.m.	n.m.	2.1	0.42	17	0.79	0.4	30.5	7.1	2.4	0.1	5.1	5	580	n.m.	1	0..29	n.m.	n.m.	66.5
CF28	1999	I	0.05–0.5	n.m.	n.m.	n.m.	n.m.	2.8	0.57	0.76	0.3	0.5	7.32	4.1	3.1	0.1	6.7	5	6.9	n.m.	8.1	1.3	n.m.	n.m.	26.3
CF30	1999	I	n.m.	40	n.m.	6.6	n.m.	2.1	0.3	14	0.24	0.3	30.5	3.6	1.7	0.1	5.2	8.8	420	n.m.	1	0.54	n.m.	n.m.	58.5
CF31	1999	I	0.5–2	39	7.4	6.9	n.m.	1.6	0.36	16	0.41	0.63	30.5	3.1	3.5	0.1	3.8	27	180	n.m.	15	0.99	n.m.	n.m.	60.2
SC09	1999	II	0.05–0.5	572	9.8	6.4	n.m.	13	4.5	70	10.2	1.3	286.8	60.9	0	0	15.4	48	3170	n.m.	3035	490	n.m.	n.m.	468.8
SC26	1999	I	0.5–2	n.m.	n.m.	n.m.	n.m.	1.1	0.4	24	2.2	0.2	51.26	9.5	1.3	0.1	2.7	5	10	n.m.	68	1.5	n.m.	n.m.	92.8
SC27	1999	I	0.5–2	n.m.	n.m.	n.m.	n.m.	1.3	0.35	14	0.84	0.2	30.5	4.1	2.3	0.17	1.3	5	3.7	n.m.	21	1.7	n.m.	n.m.	55.1
SC28	1999	I	2–10	n.m.	n.m.	n.m.	n.m.	1.5	0.35	19	0.29	0.2	41.49	2.3	1	0.1	2	5	8.3	n.m.	1	0.71	n.m.	n.m.	68.2
CB100	2000	I	0.5–2	54	9.6	7.05	374	1.37	0.54	9.55	1.62	0.14	27.45	5.9	0.74	n.m.	3.7	n.m.	<3	<10	2420	<1	<10	53	53.1
CB111	2000	I	2–10	41	7.1	6.91	308	0.7	0.89	28.2	0.54	0.07	36.6	3.81	2.26	n.m.	1.8	n.m.	4	13.2	<1	6	<10	60	65.6
CB116	2000	III	0.5–2	92	9.2	7.79	317	0.34	0.15	5.7	8.58	0.3	67.1	3.7	1.68	n.m.	5.3	n.m.	4	<10	<1	<1	<10	10	122.8
CB117	2000	III	0.5–2	90	8.7	7.3	326	0.26	0.17	3.46	9.34	0.79	64.05	3.19	1.67	n.m.	6.2	n.m.	<3	<10	<1	<1	<10	<10	88.2
CR05	2000	I	n.m.	179	10.9	7.42	295	0.7	2.62	35	2.1	0.34	122	5.01	1.56	n.m.	2.9	n.m.	50	<10	<1	<1	<10	90	172.3
CR07	2000	II	n.m.	52	8.8	6.48	333	1.73	1.16	5.36	1.33	0.11	18.3	11.2	1.21	n.m.	3.1	n.m.	4	<10	<1	<1	<10	37	43.4
CR27	2000	I	2–10	n.m.	3.3	7.35	304	0.74	1.31	12.1	2.75	0.04	51.85	6.8	3.7	n.m.	2.3	n.m.	29	<10	<1	<1	<10	50	81.4
CR30	2000	I	2–10	13	4.7	6.46	356	0.46	0.4	1.24	0.2	0.004	6.1	1.8	1.55	n.m.	1.6	n.m.	14	<10	<1	<1	<10	40	19.4
CR53	2000	I	1–2	18	2.6	7.28	284	0.86	0.45	7	0.42	0.06	21.35	2.27	3	n.m.	2.2	n.m.	<3	<10	<1	<1	<10	<10	37.4
CR55	2000	II	2–10	85	8.3	6.51	345	5.77	1.19	7.9	1.32	7.38	35.55	7.3	2.5	n.m.	3.3	n.m.	10	30	1	<2	20	60	72.3
CR79	2000	I	n.m.	10	8.9	7.25	295	1.18	1.59	8.3	2.1	0.14	44.73	8.76	2.95	n.m.	2.1	n.m.	9	<10	<1	<1	<10	40	71.8
CR81	2000	I	n.m.	n.m.	n.m.	n.m.	n.m.	0.36	0.57	16.7	6.63	0.2	73.21	10.1	2.51	n.m.	1.1	n.m.	20	<10	<1	<1	<10	70	111.4
SC01	2000	I	0.1	338	7.6	5.53	141	5.55	1.35	78.7	6.15	2.85	254.2	6.3	0	n.m.	5.6	n.m.	50	10	1350	710	20	220	363.5
SC04	2000	II	0.053	2710	6.9	5.92	−12	398	22.3	205	24.1	442	890.6	119	0	2.86	14.1	n.m.	41	3000	10,600	2230	2100	2180	2135
SC33	2000	I	3	58	4.9	7.27	307	0.78	0.7	8	1.47	0.13	34.56	7.35	1.24	n.m.	1.9	n.m.	25	<10	<1	<1	<10	50	56
SC49	2000	I	2–10	207	3.9	7.97	294	0.39	1.1	35.5	3.79	0.11	110.8	21.3	1.21	n.m.	1.5	n.m.	10	<10	<1	<1	<10	350	175.9
SC52	2000	II	n.m.	236	6.7	6.59	35	10.2	2.16	23.5	3.07	7.1	130.1	10	0	n.m.	6.4	n.m.	77	76	6380	2500	50	170	201.7
SC55	2000	I	2–10	40	2.5	6.68	343	0.87	1.07	20.1	0.5	0.28	38.63	3.01	2.01	n.m.	2.2	n.m.	39	<10	30	20	<10	30	68.6
SC62	2000	I	2–10	55	6.5	7.13	372	0.38	0.31	7.42	0.66	0.1	27.45	2.52	0.95	n.m.	0.9	n.m.	20	<10	<1	<1	10	35	40.5

Table 5
Saturation indices S.I. (= log IAP/K_{eq}, where IAP: Ion Activity Product; K_{eq}: Solubility Product), calculated with WATEQ4F for water samples

Sample	Ankerite $Ca(Fe_{0.5}Mg_{0.5})(CO_3)_2$	Calcite $CaCO_3$	Dolomite $CaMg(CO_3)_2$	Siderite $FeCO_3$	Gypsum $CaSO_4*2H_2O$	Barite $BaSO_4$	Hematite Fe_2O_3	Goethite $Fe_2O_3*H_2O$	$Fe(OH)_3$ $Fe(OH)_3$	Chalcedony SiO_2
CB100	−4.103	−2.101	−4.859	−1.674	−3.383		20.312	9.189	3.876	−0.528
CB111		−1.817	−5.288		−3.151	−1.827				−0.815
CB116		−1.056	−1.829		−3.859	−1.881				−0.357
CB117		−1.941	−3.354		−4.122					0.305
CR05		−0.540	−2.165		−3.004	−0.751				−0.604
CR07		−2.729	−5.965		−3.339	−1.336				0.558
CR27		−1.515	−3.688		−3.228	−0.600				−0.647
CR30		−3.952	−8.683		−4.698	−1.420				−0.809
CR53		−2.198	−5.647		−3.884					−0.638
CR55	−5.737	−2.622	−5.933	−3.393	−3.378	−1.131	13.352	5.713	0.452	−0.508
CR79		−1.753	−4.004		−3.282	−1.115				−0.721
SC01	−3.830	−1.871	−4.777	−1.510	−2.668	−0.702	4.176	1.126	−4.107	−0.227
SC04	−1.325	−0.753	−2.396	−0.026	−1.331	0.121	2.141	0.111	−5.095	0.0200
SC33		−1.919	−4.554		−3.350	−0.641				−0.745
SC49		−0.155	−1.282		−2.366	−0.690				−0.850
SC52	−2.530	−1.591	−4.010	0.008	−2.868	−0.176	8.125	3.104	−2.093	−0.209
SC55	−5.065	−2.114	−5.864	−2.839	−3.365	−0.807	14.682	6.393	1.369	−0.645
SC62		−2.151	−5.301		−3.832	−1.214				−1.186

Saturation indices were only calculated for samples collected in 2000, as in the 1999 campaign the pH, alkalinity and Eh were not determined in the field. Thermodynamic calculations were performed using the WATEQ4F database included in the PHREEQCI code (Parkhurst and Appelo, 1999). The most important results are reported in Table 5. Waters are undersaturated with respect to all carbonates, with the exception of samples SC04 and SC52 which are saturated with respect to siderite as well as to barite. The highest saturation relative to calcite is observed for sample SC49.

Dissolved gases were only analysed for in sample SC04 (Table 6), as it shows the highest TDS value and a natural effervescence. The gas mixture appears to be composed of more than 90% CO_2, followed by N_2 and traces of Ar, O_2 and CH_4.

Table 6
Dissolved gas analysis (sample SC04)

Dissolved gas	Concentration (mmol mol^{-1})	Concentration (%)
CH_4	0.6	0.1
CO_2	905.3	91
Ar	1.6	0.2
O_2	1.2	0.1
N_2	91.3	9

4.2.2. Isotopic data

Selected water samples were analysed for δ^2H, $\delta^{18}O$ and $\delta^{13}C$ of dissolved inorganic C (Table 7).

The $\delta^{18}O$ and δ^2H values range from −8.89 to −12.67‰ and from −59.4 to −89.3‰ SMOW respectively. In the δ^2H vs $\delta^{18}O$ plot (Fig. 5), all samples fit closely to the Global Meteoric Water Line (GMWL; Rozanski et al., 1993). The ^2H excess (13.6‰) calculated by linear regression of the data is similar to the value found for other Alpine recharged groundwaters (Carrozza et al., 1995). No correlation with the spring altitude is observed. Sample SC04 is most depleted in heavy isotopes.

Table 7
Stable isotope composition of selected water samples

Sample	δ^2H ‰ SMOW	$\delta^{18}O$ ‰ SMOW	$\delta^{13}C_{(DIC)}$ ‰ PDB
CB116	−63.2	−9.22	–
CB117	−65.0	−9.51	–
CR27	−66.7	−10.39	–
CR30	−62.4	−9.50	−23.58
CR53	−62.9	−9.47	−14.02
CR55	−72.2	−10.48	–
CR81	−59.4	−8.89	–
SC01	−82.0	−11.50	−5.55
SC04	−89.3	−12.61	−7.99
SC55	−73.3	−10.77	−4.76
SC62	−77.3	−11.23	−7.99

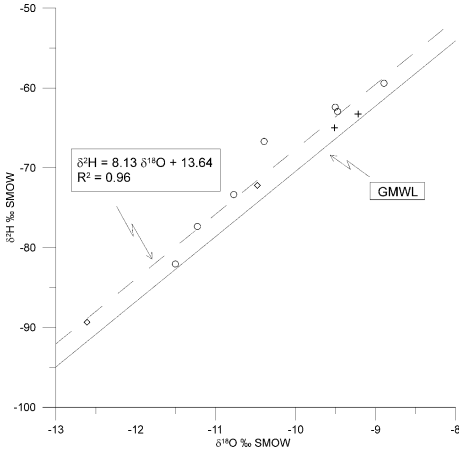

Fig. 5. δ^2H vs. $\delta^{18}O$ plot of water samples. Open circles = Type I waters; open diamonds = Type II waters; crosses = Type III waters.

The $\delta^{13}C$ values of DIC range from −23.6 to −4.6‰ PBD. The presence of highly negative values, together with high dissolved CO_2 content, will be discussed in detail to constrain the origin of the gas.

Tritium was only analysed for in sample SC04, the most saline water, in order to check for the presence of highly mineralised, long-resident groundwaters. The result of 10.3 ± 1.3 TU provides evidence that this water was recharged in the past few decades and suggests limited, if any, mixing with old fluids from depth.

5. Discussion

5.1. Constraints on the origin of fracture filling carbonates

At present, the origin of the carbonate fracture fillings is in general poorly constrained, as thorough petrologic studies of the hydrothermal systems are missing. The study shows that carbonate fillings are related to multi-stage circulation of hydrothermal fluids along E–W and NW–SE fracture systems, which are part of a transtensional shear zone. The P–T conditions of the hydrothermal system are so far not known; however, the geological and petrographical data presented here (structural setting; vein assemblages and textures; hydrothermal alteration) suggest a mesothermal character (i.e. T ~ 200–350 °C, $P_{fluids} > P_{hydrostatic}$). No data on the fluid composition are available from the literature, and a separate fluid inclusions study is in progress. Preliminary results show abundant two phase (liquid + vapour) inclusions in all carbonate ± quartz assemblages, i.e. dominantly aqueous fluids with low CO_2 content and low to moderate salinity. The same typology of fluid inclusions occurs in other siderite-rich districts, from the Italian Western Alps (Lanzo Valleys, Piemonte Zone; Rossetti, unpublished data) and Bohemian Massif (Hein, 1993). Besides the aqueous two-phase inclusions, H_2O–CO_2 3-phase inclusions (liquid H_2O + liquid CO_2 + vapour) were occasionally found within the previously mentioned quartz ± sulphide veinlets.

In the Western Alps, late-alpine hydrothermal veins occur from the Simplon dome to the Lanzo Valleys, mainly located in the axial sector of the belt. North of the Gran Paradiso Massif, they consist of mesothermal quartz-Au lodes, recently studied in great detail, particularly by Diamond and co-workers (Diamond, 1990; Pettke and Diamond, 1997; Pettke et al., 1999, 2000, and references therein). Mainly on the basis of fluid inclusions, radiogenic isotopes and geochronological data, it was suggested that "the ore-bearing fluid was produced by a 20 Ma history of prograde metamorphic devolatilization of calc-schists at depth". The age trend of mineralisation would reflect "the continuous ascent of fluid and vein formation in retrograding rocks during extreme differential uplift and denudation of the Alpine orogenic wedge" (Pettke et al., 1999). Compared to these Au veins, the studied fracture fillings show a number of similarities, which include the tectonic setting, the mesothermal character, and the strong Au enrichment. Differences are the vein assemblages (namely, the carbonate-rich gangue and the high content of sulphides and sulphosalts, often Sb-rich) and the mostly aqueous composition of parental fluids. On the other hand, the veins in question are quite similar (tectonic setting; siderite-rich gangue assemblages; texture; mesothermal character; fluid inclusions typologies) to the siderite hydrothermal bodies from the Lanzo Valleys (Castelli et al., 1995; Rossetti, unpubl. data).

The data acquired so far do not allow unambiguous discrimination between possible fluid sources. Based on the above mentioned similarities with the quartz–Au deposits to the north, a relationship with metamorphic fluids would also seem likely for the Orco Valley veins. The discrepancies mentioned between the two vein systems may be due to different P–T conditions and fluid source(s). In the metamorphic devolatilization working hypothesis the composition of the Orco Valley vein fillings requires an external source for fluids, which must be located underneath the Gran Paradiso Massif.

Isotopic data can provide additional constraints to the genetic models, although the lack of a precise formation temperature for these deposits precludes a conclusive discussion. Assuming a deposition temperature between 200 and 350 °C (typical mesothermal conditions) and using the published isotopic fractionation factors of Bottinga (1969), Carothers et al. (1988) and Deines et al. (1974), the $\delta^{13}C$ of CO_2 in equilibrium with

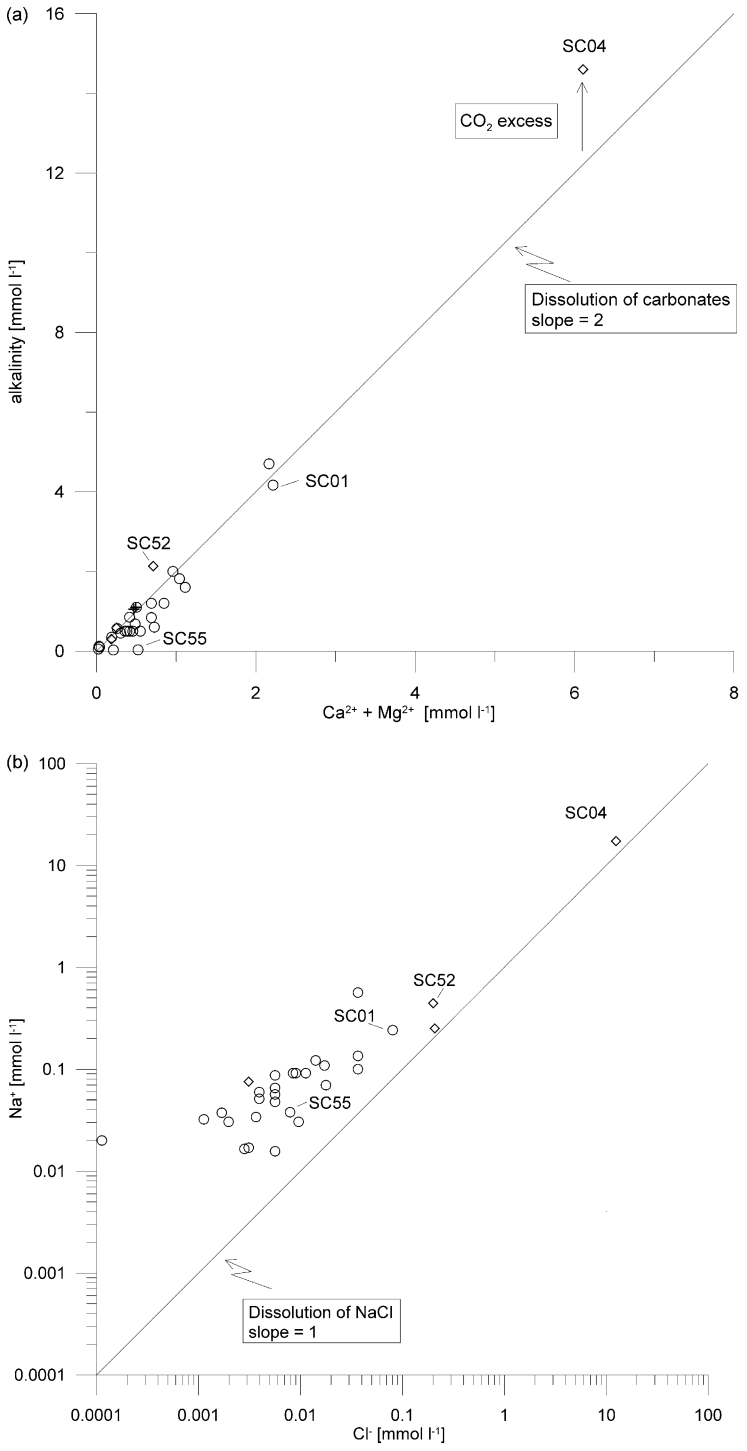

Fig. 6. Correlations between major ions in groundwaters: (a) alkalinity vs. Ca + Mg; (b) Na vs. Cl. Open circles = Type I waters; open diamonds = Type II waters; crosses = Type III waters.

siderite (Table. 3) would be in the range of −13.9 to −9 ‰. Hydrothermal fluids originated from, or interacted with the graphitic schists of the Internal Briançonnais Units, which underlie the Gran Paradiso Massif according to the crustal cross-section of Marchant and Stampfli (1997), based on the ECORS-CROP deep seismic traverse (Bayer et al., 1987), can account for these negative $\delta^{13}C$ values. A contribution of organic carbon was also suggested for other vein (Hein, 1993) and stratiform (Cortecci and Frizzo, 1993) siderite deposits.

For the same temperature conditions, using the isotopic fractionation factors of Carothers et al. (1988) and O'Neil et al. (1969), the oxygen isotopic composition of the fluid precipitating siderite would range from +8.9 to +15.1‰ SMOW. These values fall within the range generally shown by phanerozoic mesothermal deposits, including orogenic Au lodes, and are consistent with, even if not diagnostic of, a metamorphic fluid origin (Ridley and Diamond, 2000, and references therein).

As clearly shown by the petrographic study, calcite is not in equilibrium with siderite, but is related to a very late, low temperature stage. Disequilibrium is confirmed by the isotopic data: in fact, assuming mesothermal conditions for the calcite formation, values for the attendant fluid would be very different in $\delta^{13}C$ (−5.7 to −3.4‰) and $\delta^{18}O$ (+0.7 to +6.5). This would imply a drastic change in the source of CO_2, from organic to deep inorganic, while maintaining the same type of highly-exchanged hydrothermal fluid. Considering instead a low deposition temperature, in the 25–75 °C interval, the equilibrium isotopic values ($\delta^{13}C$: −13.8 to −10.2‰, $\delta^{18}O$: −20.2 to −11.6‰) are consistent with a meteoric fluid penetrating into the rock matrix at shallow depths and equilibrating at low temperature with the host minerals, in a geologic situation similar to the one observed today.

5.2. Origin of groundwaters and dissolved salts

Most groundwaters show characteristics of recently recharged surface waters, namely a low temperature at the outflow (<10 °C), low TDS and negative saturation

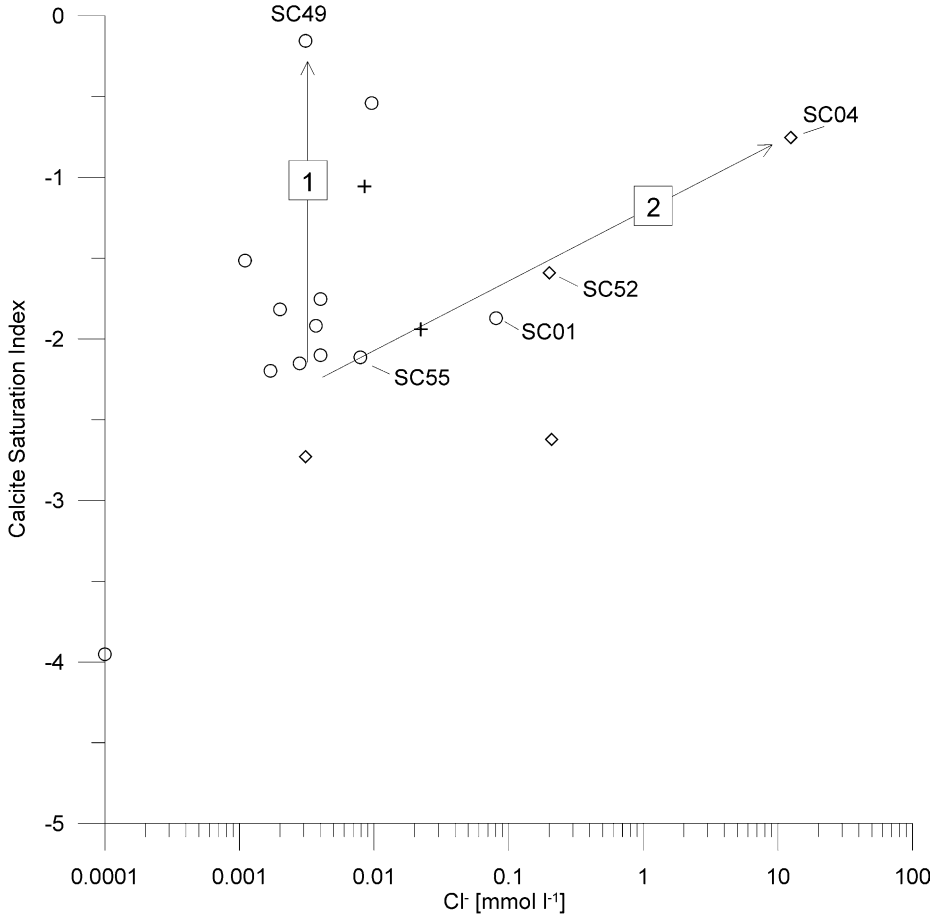

Fig. 7. Possible evolution trends of the calcite saturation as a function of the Cl content. Open circles = Type I waters; open diamonds = Type II waters; crosses = Type III waters.

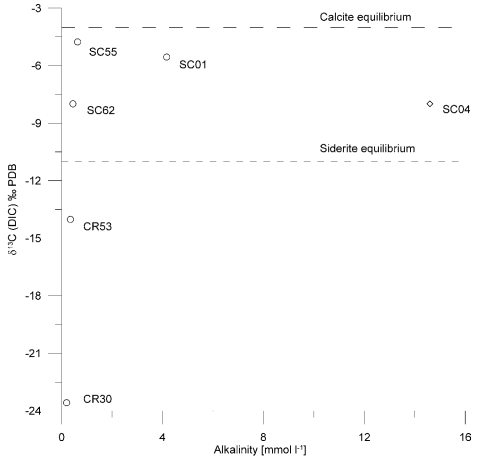

Fig. 8. DIC isotopic composition vs. alkalinity in water samples. Open circles = Type I waters; open diamonds = Type II waters.

indices with respect to silicates and carbonates, an acidic pH, positive Eh values, the presence of nitrates and a water isotopic composition falling on the GMWL.

The Ca/Mg molar ratio in groundwaters is higher than one, except in samples CB116 and CB117, in which Mg dominates. These samples belong to type III groundwaters, outflowing in a limited portion of the studied area, where the substratum is composed of serpentinites (Fig. 2). Recently, the evolution of groundwaters circulating in this type of Mg-bearing silicate rocks was extensively discussed by Bruni et al. (2002).

The circulation of all the other groundwaters is restricted to gneiss. Nevertheless, in some sectors of the region studied, carbonate fillings are found in fractures, which may represent preferential paths for water circulation. In the diagram of alkalinity vs. Ca + Mg (Fig. 6a), all samples tend to plot along a line with a slope of 2, that corresponds to the dissolution of Ca–Mg carbonates. This process is likely the factor controlling the chemical composition of groundwaters. Sample SC04 does not plot on this line, because of its alkalinity excess, due to the high pCO_2.

In the Na vs. Cl diagram (Fig. 6b), the most saline water samples SC01 and SCO4 align on a 1:1 slope, representative of the dissolution of NaCl. Rock leachates indicate that a large amount of Cl^- (60–90 ppm) is contained in carbonate fracture fillings, displaying the same 1:1 ratio with Na. A deviation from this trend is shown by low Cl^- waters, indicating an additional source of Na possibly from hydrolysis of silicates.

This interpretation is supported by the plot showing the calcite saturation index vs. Cl content (Fig. 7), evidencing these two separate trends:

- Trend 1, evolving towards calcite saturation at constant Cl concentration, could correspond to waters slowly equilibrating with the rock matrix (Type I waters).
- Trend 2, evolving towards calcite saturation with great increase of Cl content, includes waters which come into contact with carbonate fracture fillings (Type II waters). In order to maintain disequilibrium with carbonates, these waters must evolve in a system which is open to CO_2, as evidenced by acidic pH and dissolved gas analysis. Leaching of fluid inclusions and dissolution of carbonate fillings would then account for their high TDS and Cl contents.

5.3. Origin of dissolved CO_2

Indications of the origin of dissolved inorganic carbon (DIC) in groundwaters can be obtained from isotopic data. In Fig. 8, the relationship between the isotopic composition of DIC and alkalinity is shown. Samples CR30, CR53, SC62 and SC55 are representative of groundwaters evolving from isotopic equilibrium of DIC with soil-derived CO_2 (−23 to −15 δ‰ PDB, Clark and Fritz, 1997) to equilibrium with calcite from fracture fillings, and their log pCO_2 values range from −3 to −1.5, as usually found in recent groundwaters and in surface waters. This inferred evolution is typical of shallow groundwaters in granitic environments, where uptake of soil CO_2 and calcite dissolution control the hydrochemical evolution (Fritz et al., 1989). Sample SC55 is closest to isotopic equilibrium with calcite in fracture fillings, with a measured value of $\delta^{13}C = -3.97$‰.

Samples SC01 and SC04 instead display more depleted isotopic values and an increase in log pCO_2 (up to −0.02). The isotopic equilibrium with calcite is displaced and samples are close to siderite isotopic equilibrium, calculated using the siderite–CO_2 fractionation factors reported by Carothers et al. (1988).

As already mentioned, Type II waters must evolve in a system which is open to CO_2. The DIC composition of sample SC04 is in equilibrium with a $\delta^{13}C_{CO_2}$ of −18.0 ‰ PDB (calculated using the fractionation factors published by Mook et al., 1974). It could be argued that this value reflects low temperature equilibration with solid carbonates, displaying negative C isotopic compositions, rather than an input of deep CO_2. Geochemical modelling of these groundwaters was then attempted to evaluate the relative contribution of dissolved CO_2 and carbonate fracture fillings to the isotopic composition of DIC.

5.4. Geochemical modelling

In granitic environments, several models are available to describe the water–rock interaction processes at low

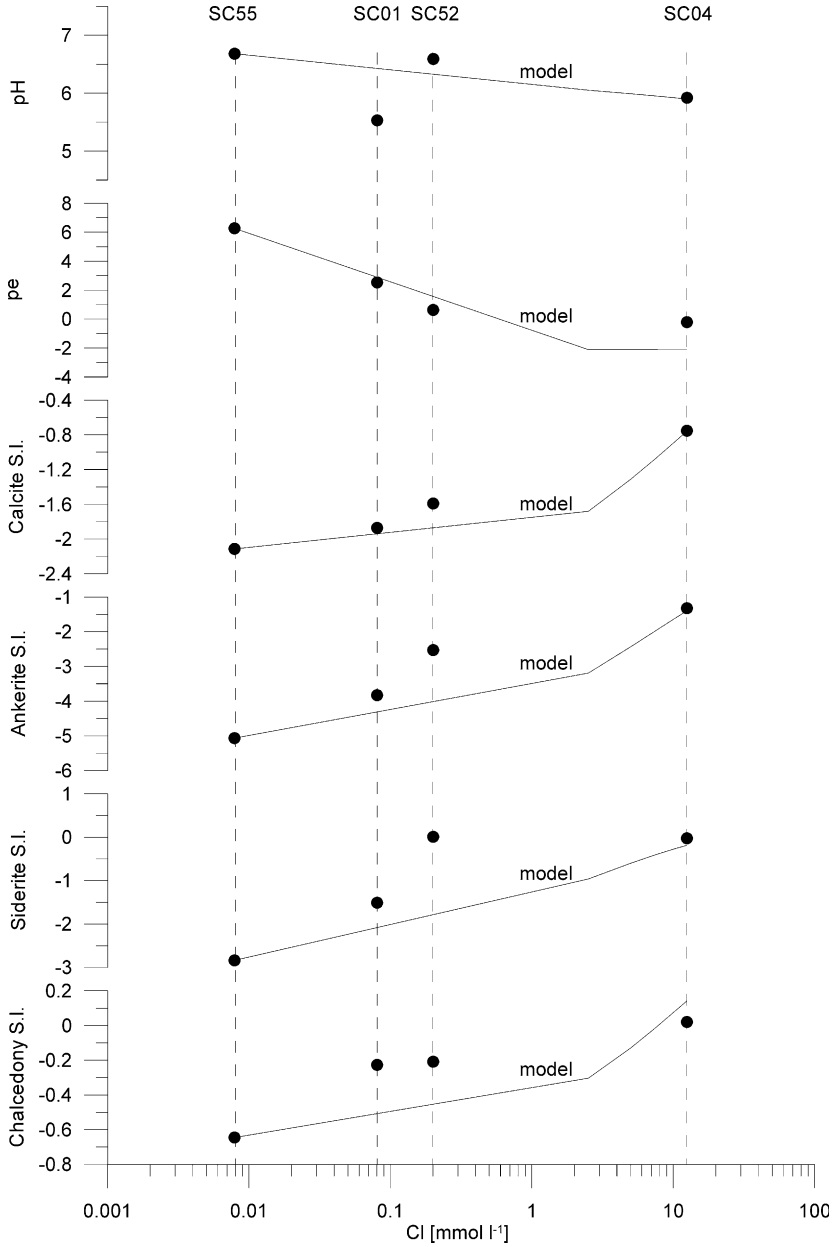

Fig. 9. Comparison between modelled groundwater evolution and water samples.

temperatures (Grimaud et al., 1990; Michard et al., 1996; Beaucaire et al., 1999; Gascoyne and Wikberg, 1999; Kraynov and Ryzhenko, 2000). These models normally consider waters in equilibrium with rock forming minerals, i.e. with long residence times.

In the present case, the waters are not in equilibrium with the rock. An additional problem is the lack of thermodynamic data for simulating the dissolution of non-stoichiometric ankerite. Al et al. (2000) calculated the dissolution constant, log K, considering ankerite as a solid solution between the two end-members, $CaMg(CO_3)_2$ and $CaFe(CO_3)_2$, with known thermodynamic properties (Wogelius et al., 1992). Using this approach log K was recalculated for the mean composition of ankerite Ca $(Fe_{0.5}Mg_{0.5})$ $(CO_3)_2$. The calculated value of $= -18.17$ at 25 °C is close to those reported in the literature (Morse and Mackenzie, 1990) for stoichiometric ankerite dissolution (−19.92) and dolomite dissolution (−17.09), but very different from that reported for siderite dissolution (−10.50).

In the water–rock interaction modelling two computer codes were used.

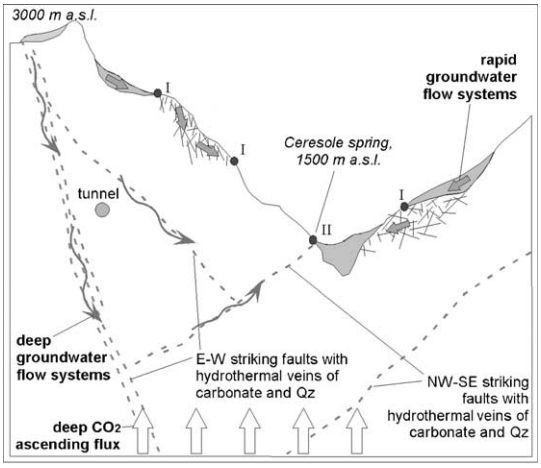

Fig. 10. Conceptual model of present groundwater circulation in the Orco Valley. I = Type I outflows, II = Type II outflows. The approximate location of the planned hydroelectric diversion tunnel is also shown.

Inverse modelling was performed using the NETPATH code (Plummer et al., 1994). Sample SC55 was selected as "initial water" and SC04 as "final water". Constraints include Ca, Fe, Mg, Mn, S, C, Si, Cl and K. Mineral phases which are known to be present in the rocks, and could account for the groundwater hydrochemical evolution are calcite, ankerite (mean composition Ca $(Fe_{0.5}Mg_{0.5})$ $(CO_3)_2$), siderite (mean composition $Fe_{0.85}Mg_{0.1}Mn_{0.05}CO_3$), pyrite, halite, albite, K-feldspar, SiO_2 and CO_2 gas, each of those constraining an element. None of these phases were forced in the system and both dissolution and precipitation were allowed.

Based on the saturation indices with respect to the different phases, the quantitative description of the evolution of Type II groundwater implies the dissolution of CO_2 gas, carbonates, halite, pyrite, K-feldspar, and the precipitation of goethite and silica, according to the equation:

$$\begin{aligned} &\mathrm{SC55} + 51.4\,\mathrm{CO_2} + 2.64\,\mathrm{Calcite} + 1.98\,\mathrm{Ankerite} \\ &\quad + 0.013\,\mathrm{Siderite} + 12.5\,\mathrm{Halite} + 0.6\,\mathrm{Pyrite} \\ &\quad + 0.54\,\mathrm{K\text{-}feldspar} \\ &\quad = \mathrm{SC04} + 1.39\,\mathrm{Goethite} + 1.43\,\mathrm{SiO_2} \end{aligned}$$

The computer code PHREEQCI (Parkhurst and Appelo, 1999) was used for forward modelling. i.e. the phases with their relative stoichiometry were progressively added to SC55 in 5 steps, and the calculated evolution and "final water" were compared with the composition of sampled waters. Goethite and SiO_2 were allowed to precipitate.

The model adequately describes the pH and redox potential (pe) distribution, and the saturation indices relative to carbonate minerals (calcite, ankerite, siderite) and silica species (Fig. 9), although some discrepancies appear. This is possibly due to the erratic input of CO_2 and to the non-homogeneous Cl distribution in the fracture fillings, both factors not appropriately represented by the progressive addition of the above reaction.

Similar models were evoked by Benvenuti et al., (2000) and Al et al. (2000) to describe the evolution of groundwater composition during weathering of sulphide-rich mine tailings in surface and subsurface environments.

Given the large amount of dissolved CO_2, in Type II waters the isotopic composition of DIC is clearly imposed by the CO_2 gaseous phase. Therefore, the assumption of a system which is open to a deep CO_2 flux with an important organic contribution is verified.

Finally, the Cl concentration difference between the initial (SC55) and the final (SC04) water composition is of 12.5 mmol l^{-1}, compared with 2 mmol kg^{-1} of Cl^- in fracture fillings. This would imply that each litre of water completely leached about 6 kg of vein material to acquire the observed chemical composition. This value could be slightly overestimated, as rock samples were collected close to the surface, and the Cl content of the rock might be greater at depth. Nevertheless, this points to a relatively low water to rock ratio in the subsoil, as testified also by the low discharge rate.

6. Conclusion

The methodology adopted in this study represents a rather unconventional approach in pre-feasibility studies for underground designs and construction works. The mineralogical and geochemical study of fracture fillings, combined with the hydrochemical characterisation of groundwater, allowed the definition of a hydrogeological and geochemical model, identifying potential contributions from deep fluids and factors controlling groundwater chemical composition.

On this basis two main types of groundwater flow systems were distinguished (Fig. 10):

1. rapid groundwater flow systems, developed both in the weathered zone of the Massif near the surface and in thin Quaternary deposits, which feed most of the springs observed in the valley; and
2. deep groundwater flow systems, recently recharged by descending waters up to depths of more than a hundred meters, flowing in faults in the rock basement.

This second type of groundwater outflows in a sector delimited by two E–W through-going shear zones and associated syngenetic Riedel NW–SE faults. They dis-

play peculiar hydrochemical features such as an acidic pH, and high Cl^- and dissolved CO_2 contents, all maintaining a highly aggressive character with respect to the host rock. Consequently, the location of new diversion tunnels and powerhouse caverns in this zone is strongly discouraged.

The dissolved CO_2 isotopic composition of these waters testifies to a clear organic C contribution which could be related to the decomposition of, or the interaction with, graphitic schists at depth. In the past, similar CO_2-bearing fluids were considered responsible for the formation of Fe-bearing carbonate fracture fillings. The persistence through time of an organic CO_2 flux in the region has implications for the reconstruction of the Alpine tectonic evolution and deep structure. For this reason, the observed shift towards more depleted C isotopic compositions, as reconstructed from the comparison between present dissolved inorganic C data and carbonate fracture filling composition, should be investigated in the future. CO_2-rich hydrothermal and low-temperature springs are common in the Alps, and the study of their occurrence, geologic setting and isotopic composition could help in identifying similar fluid sources and upwelling mechanisms.

Acknowledgements

Aldo Fiamberti supported the project on behalf of AEM Torino, and Marco Rubbo, from the University of Torino, Italy, helped us in thermodynamic calculations. Catherine Beaucaire, from IRSN, France, Gianni Cortecci, form the University of Bologna, Italy, and Gian Maria Zuppi from the University of Venezia, Italy are acknowledged for their thoughtful revision and constructive criticism of the first draft of the manuscript.

References

Al, T.A., Martin, C.J., Blowes, D.W., 2000. Carbonate-mineral/water interactions in sulphide-rich mine tailings. Geochim. Cosmochim. Acta 64, 3933–3948.

Al-Aasm, I., Taylor, B.E., South, B., 1990. Stable isotope analysis of multiple carbonate samples using selective acid extraction. Chem. Geol. (Isotope Geosci. Sect.) 80, 119–125.

Bayer, R., Cazes, M., Dal Piaz, G.V., Damotte, B., Elter, G., Gosso, G., Alfred, H., Lanza, R., Lombardo, B., Mugnier, J.L., Nicolas, A., Nicolich, R., Polino, R., Roure, F., Sacchi, R., Scarascia, S., Tabacco, I., Tapponnier, P., Tardy, M., Taylor, M., Thouvenot, F., Toreilles, G., Villien, A., 1987. Premier résultats de la traversée des Alpes occidentales par sismique reflexion verticale (Programme ECORS-CROP). C. R. Acad. Sci. Paris 305, 1461–1470.

Beaucaire, C., Gassama, N., Tresonne, N., Louvat, D., 1999. Saline groundwaters in the hercynian granites (Chardon Mine, France): geochemical evidence for the salinity origin. Appl. Geochem. 14, 67–84.

Benvenuti, M., Mascaro, I., Corsini, F., Ferrari, M., Lattanzi, P., Parrini, P., Costagliola, P., Tanelli, G., 2000. Environmental mineralogy and geochemistry of waste dumps at the Pb(Zn)–Ag Bottino mine, Apuane Alps. Italy. Eur. J. Mineral 12, 441–453.

Blyth, A., Frape, S., Blomqvist, R., Nissinen, P., 2000. Assessing the past thermal and chemical history of fluids in crystalline rock by combining fluid inclusion and isotopic investigations of fracture calcite. Appl. Geochem. 15, 1417–1437.

Bottinga, Y., 1969. Calculated fractionation factors for carbon and hydrogen isotope exchange in the system calcite–CO_2–graphite–methane–hydrogen and water vapor. Geochim. Cosmochim. Acta 33, 49–64.

Bruni, J., Canepa, M., Chiodini, G., Cioni, R., Cipolli, F., Longinelli, A., Marini, L., Ottonello, G., Vetuschi Zuccolini, M., 2002. Irreversible water–rock mass transfer accompanying the generation of the neutral, Mg–HCO_3 and high-pH, Ca–OH spring waters of the Genova province. Italy. Appl. Geochem 17, 455–474.

Carothers, W.W., Adami, L.H., Rosenbauer, R.J., 1988. Experimental oxygen isotope fractionation between siderite–water and phosphoric acid liberated CO_2–siderite. Geochim. Cosmochim. Acta 52, 2445–2450.

Carrozza, D., Novel, J.P., Pollicini, F., 1995. Caractérisation hydrodynamique, hydrochimique et isotopique de quelques aquifères des massifs entourant la plaine alluviale d'Aoste, 2° IMYRAG, Peveragno (CN), 11–13 October.

Castelli, D., Clerico, F., Rossetti, P., 1995. Mineralizzazioni ad arseniuri di cobalto e nichel nelle metaofioliti delle Alpi Occidentali: petrografia e aspetti giacimentologici preliminari. Congr. Soc. It. Mineral. Petrol., Venezia, Plinius 14, 107–108.

Cevales, G., 1961. I giacimenti minerari del Gran Paradiso. Rend. Soc. Min. It. 42, 193–217.

Clark, J., Fritz, P., 1997. Environmental Isotopes in Hydrology. Lewis Publishers, CRC Press, Boca Raton.

Clauer, N., Frape, S., Fritz, P., 1989. Calcite veins of the Stripa granite (Sweden) as records of the origin of the groundwaters and their interactions with the granitic body. Geochim. Cosmochim. Acta 53, 1777–1781.

Coleman, M.L., Sheppard, T.J., Durham, J.J., Rouse, J.E., Moore, G.R., 1982. Reaction of water with zinc for hydrogen isotope analysis. Anal. Chem. 54, 993–995.

Compagnoni, R., Elter, G., Lombardo, B., 1974. Eterogeneità stratigrafica del complesso degli "gneiss minuti" nel massiccio cristallino del Gran Paradiso. Mem. Soc. Geol. It. 13, 227–239.

Compagnoni, R., Prato, R., 1969. Paramorfosi di cianite su sillimanite in scisti pregranitici del Massiccio del Gran Paradiso. Boll. Soc. Geol. It. 88, 537–549.

Conti, A., Turpin, L., Polino, R., Mattei, M., Zuppi, G.M., 2001. The relationship between evolution of fluid chemistry and the style of brittle deformation: examples from the Northern Apennines (Italy). Tectonophys. 330, 103–117.

Cortecci, G., Frizzo, P., 1993. Origin of siderite deposits from the Lombardy Valleys, northern Italy: a carbon, oxygen and strontium isotope study. Chem. Geol. (Isotope Geosci. Sect.) 105, 293–303.

Craig, H., 1957. Isotopic standards for carbon and oxygen and correlation factors for mass spectrometric analysis of carbon dioxide. Geochim. Cosmochim. Acta 12, 133–149.

Dal Piaz, G., Lombardo, B., 1986. Early Alpine eclogite metamorphism in the Penninic Monte Rosa- Gran Paradiso

basement nappes of the northwestern Alps. Mem. Geol. Soc. Am. 164, 249–265.

Deines, P., Langmuir, D., Harmon, R.S., 1974. Stable carbon isotope ratios and the existence of a gas phase in the evolution of of carbonate ground waters. Geochim. Cosmochim. Acta 38, 1147–1164.

Delle Piane, L., Dematteis, A., Perello, P., Fiamberti, A., 2001a. The geological study: "back to the past" as an innovative approach to preliminary feasibility studies for underground hydro-power plants in alpine environment. In: AITES-ITA 2001 World Tunnel Congress, Milano, 10–13 June, vol. 1, pp. 249-256.

Delle Piane, L., Perello, P., Damiano, A. 2001b. Ductile structural setting of the Gran Paradiso Unit and relationships with large scale landslides in the Orco Valley (Italian Western Alps). "Convegno in memoria di Giulio Elter", Cogne, 21–22 June.

Diamond, L.W., 1990. Fluid inclusion evidence for P-V-T-X evolution of hydrothermal solutions in Late-Alpine gold-quartz veins at Brusson, Val d'Ayas, NW Italian Alps. Am. J. Sci. 290, 912–958.

Epstein, S., Mayeda, T.K., 1953. Variations of the $^{18}O/^{16}O$ ratio in natural waters. Geochim. Cosmochim. Acta 4, 213–224.

Fritz, S.J., 1994. A survey of charge-balance errors on published analyses of potable ground and surface water. Groundwater 32, 539–546.

Fritz, P., Fontes, J.Ch., Frape, S.K., Louvat, D., Michelot, J.L., Balderer, W., 1989. The isotope geochemistry of carbon in groundwater at Stripa. Geochim. Cosmochim. Acta 53, 1765–1775.

Gascoyne, M., Wikberg, P., 1999. Geochemistry of the Äspö Hard Rock Laboratory, Sweden. Appl. Geochem. 14, 962.

Grimaud, D., Beaucaire, C., Michard, G., 1990. Modelling of the evolution of groundwaters in a granite system at low temperature: the Stripa groundwaters, Sweden. Appl. Geochem. 5, 515–525.

Hein, U.F., 1993. Synmetamorphic Variscan siderite mineralisation of the Rhenish Massif, Central Europe. Mineral. Mag. 57, 451–467.

Jäckli, H., 1970. Kriterien zur Klassifikation von Grundwasservorkommen. Eclogae Geol. Helv. 63, 389–434.

Kraynov, S.R., Ryzhenko, B.N., 2000. A thermodynamic geochemical model describing the formation of chloride, carbonate, and sulfate waters in crystalline massifs and the causes of geochemical zoning of these waters. Geochem. Internat. 38, S173–S185.

Kroopnick, P., 1974. The dissolved O_2-CO_2-^{13}C system in the eastern equatorial Pacific. Deep-Sea Res. 21, 211–227.

Marchant, R.H., Stampfli, G.M., 1997. Crustal and lithospheric structure of the Western Alps: geodynamic significance. In: Pfiffner, O.A., Lehner, P., Heitzmann, P., Mueller, S., Steck A. (Eds.), Deep Structure of the Swiss Alps, Basel. pp. 326–337.

Michard, G., Pearson, F.J., Gautschi, A., 1996. Chemical evolution of waters during long term interaction with granitic rocks in northern Switzerland. Appl. Geochem. 11, 757–774.

Mook, W.G., Bommerson, J.C., Staverman, W.H., 1974. Carbon isotope fractionation between dissolved bicarbonate and gaseous carbon dioxide. Earth Planet. Sci. Lett. 22, 169–176.

Morse, J.W., Mackenzie, F.T., 1990. Geochemistry of Sedimentary Carbonates. Developments in Sedimentology, 48. Elsevier, Amsterdam.

O'Neil, J.R., Clayton, R.N., Mayeda, T.K., 1969. Oxygen isotope fractionation in divalent metal carbonates. J. Chem. Phys. 51, 5547–5558.

Parkhurst, D.L., Appelo, C.A.J., 1999. User's guide to PHREEQC (Version 2)- A computer program for speciation, batch-reaction, one-dimensional transport, and inverse geochemical calculations. U.S. Geol. Surv. Water-Resourc. Investig. Rep 99-4259, 310.

Perello, P., Delle Piane, L., Piana, F., Stella F. and Damiano, A. Brittle post-metamorphic tectonics in the Gran Paradiso Massif (north-western Italian Alps). Geodyn. Acta (submitted for publication).

Pettke, T., Diamond, L.W., 1997. Oligocene gold-quartz veins at Brusson, NW Alps: Sr isotopes trace the source of ore-bearing fluid to over 10km depth. Econ. Geol. 92, 389–406.

Pettke, T., Diamond, L.W., Villa, I., 1999. Mesothermal gold veins and metamorphic devolatilisation in the NW Alps: The temporal link. Geology 27, 641–644.

Pettke, T., Diamond, L.W., Kramers, J.D., 2000. Mesothermal gold lodes in the north-western Alps: a review of genetic constraints from radiogenic isotopes. Eur. J. Mineral. 12, 213–230.

Plummer, L.N., Prestemon, E.C., Parkhurst, D.L., 1994. An interactive code (NETPATH) for modeling NET geochemical reactions along a flow PATH-Version 2.0. U.S. Geol. Surv. Water-Resour. Investig. Rep 94-4169, 130.

Reyes, E., Pérez del Villar, L., Delgado, A., Cortecci, G., Núñez, R., Pelayo, M., Cózar, J.S., 1998. Carbonatation processes at the El Berrocal natural analogue granitic system (Spain): inferences from mineralogical and stable isotope studies. Chem. Geol. (Isotope Geosci. Sect.) 150, 293–315.

Ridley, J.R., Diamond, L.W., 2000. Fluid chemistry of orogenic lode-gold deposits and implications for genetic models. In: Hagemann, S., Brown, P.E. (Eds.), Gold in 2000, 2000. (Eds.), Rev. Econ. Geol13. , pp. 141–162.

Rosenbaum, J., Sheppard, S.M.F., 1986. An isotopic study of siderites, dolomites and ankerites at high temperatures. Geochim. Cosmochim. Acta 50, 1147–1150.

Rozanski, K., Araguás-Araguás, L., Gonfiantini, R., 1993. Isotopic patterns in modern global precipitation. In: Continental Isotope Indicators of Climate, A.G.U. Monograph.

Sacchi, E., Michelot, J.L., Pitsch, H., 2000. Porewater Extraction from Argillaceous Rocks for Geochemical Characterisation: Methods and Interpretations. OECD, NEA, Paris.

Savoye, S., Aranyossy, J.F., Beaucaire, C., Cathelineau, M., Louvat, D., Michelot, J.L., 1998. Fluid inclusions in granites and their relationships with present-day groundwater chemistry. Eur. J. Mineral. 10, 1215–1226.

SEA Consulting srl, 2001. Studio geologico-strutturale della Valle dell'Orco e dell'alto versante sinistro della Val Grande di Lanzo (TO), Unpublished Report SDP00-15-22-RGL11, Azienda Elettrica Municipale Torino, 272.

Unterweger, M.P., Coursey, B.M., Shima, F.J., Mann, W.B., 1980. Preparation and calibration of the 1978 National Bureau of Standards tritiated water standard. Int. J. Appl. Rad. Isot 3, 601–614.

Wogelius, R.A., Fraser, D.G., Feltham, D.J., Whiteman, M.I., 1992. Trace element zoning in dolomite: proton microprobe data and thermodynamic constraints on fluid compositions. Geochim. Cosmochim. Acta 56, 319–334.